INTERNATIONAL JOURNAL FOR NUMERICAL METHODS IN FLUIDS
Int. J. Numer. Meth. Fluids 2002; **40**:189–196 (DOI: 10.1002/fld.272)

Material stretching in laminar mixing flows: extended mapping technique applied to the journal bearing flow

P. D. Anderson[1,*,†], O. S. Galaktionov[1], G. W. M. Peters[1], H. E. H. Meijer[1] and C. L. Tucker III[2]

[1]*Dutch Polymer Institute, Materials Technology, Eindhoven University of Technology, 5600 MB Eindhoven, The Netherlands*
[2]*Department of Mechanical and Industrial Engineering, University of Illinois at Urbana-Champaign, Urbana, IL 61801, U.S.A.*

SUMMARY

This paper deals with chaotic mixing in the journal bearing flow. A recently developed mapping technique is used to study the dynamics of this well-known prototype mixing flow. Eigenvalues and eigenmodes of the resulting mapping matrix are used to reveal different zones of mixing. Moreover, an extension of the technique, adding an area tensor to described structure on cell level, is used to determine rate of interfacial area during mixing. The technique is shown to be consistent with the more consuming front tracking model. Copyright © 2002 John Wiley & Sons, Ltd.

KEY WORDS: Chaotic mixing; journal bearing flow; mapping method; eigenvalue analysis

1. INTRODUCTION

Time-periodic Stokes flow ($Re \ll 1$) of a viscous incompressible Newtonian fluid in the gap between two eccentric cylinders is considered. This is a well-known, experimentally realizable chaotic prototype flow extensively used for studying laminar mixing mechanisms (see for example References [1, 7]), and has been considered in classical works on lubrication theory [4, 5]. These papers describe the idealized flow between the rotating journal and its cylindrical support, when the gap is filled by lubricating fluid (hence the name 'journal bearing flow'). The fact that a chaotic flow can easily be generated by rotating the cylinders in a time-periodic fashion makes it a convenient prototype flow to study mixing phenomena.

The geometry of the flow domain is characterized by two dimensionless parameters: the ratio of the radii of the inner and outer cylinder $r_{\text{in}}/r_{\text{out}}$, and the dimensionless eccentricity $e = d/r_{\text{out}}$, where d is the distance between the centres of two cylinders. The periodic flow is induced by rotating the cylinders using a discontinuous two-step protocol: during the first

*Correspondence to: P. D. Anderson, Dutch Polymer Institute, Materials Technology, Eindhoven University of Technology, 5600 MB Eindhoven, The Netherlands.
†E-mail: p.d.anderson@tue.nl

Received May 2001
Revised October 2001

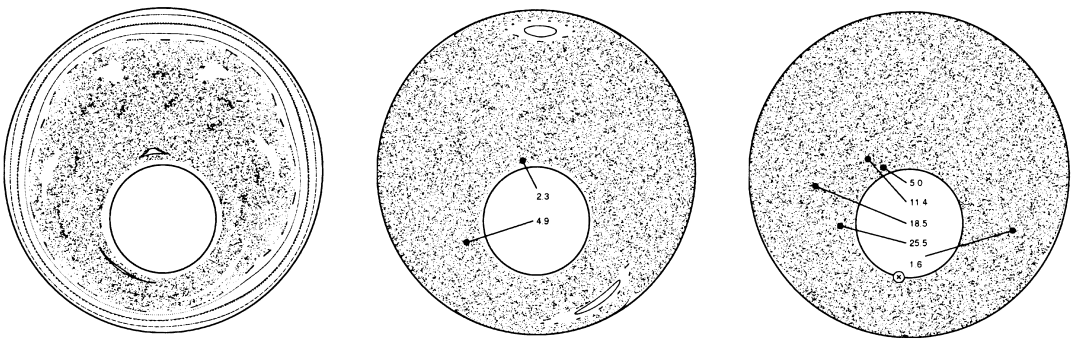

Figure 1. Examples of Poincaré maps for the flows with different values of θ: (a) $\theta = 0.5\pi$; (b) $\theta = 1.0\pi$; (c) $\theta = 2.0\pi$. The location of some first-order hyperbolic periodic points is shown by black circles. The numbers indicate the corresponding maximum stretching values.

half-period the outer cylinder is rotated while the inner remains stationary; during the second half-period the outer cylinder is fixed and inner one rotates. In the Stokes approximation the fluid motion is completely defined by the rotation angles of the cylinders. Thus, the flow protocol can be described by two dimensionless parameters: the rotation angle θ of the outer cylinder and the ratio Ω of the rotation angle of the inner cylinder to that of the outer. Following Muzzio *et al.* [7] the geometric parameters are set to $r_{\text{in}}/r_{\text{out}} = 1/3$, $c = 0.3$ and the ratio of the rotation angles is kept as $\Omega = 3.0$.

Figure 1 compares different Poincaré maps [8], providing an asymptotic picture of the mixture, and reveals chaotic and regular regions for different rotation angles. These maps are calculated by tracking a limited number of markers for many periods and plotting their position at every period. The flow with $\theta = 0.5\pi$ (Figure 1(a)) contains a large number of islands of different order and a wide ring of regular flow along the outer boundary. No first-order periodic points are present. Periodic points are points which return to their original position after one or more periods of flow. They are classified according to the nature of the stretching in their neighbourhood. Elliptic (stable) periodic points are at the centre of non-mixing regions, called islands, while hyperbolic (unstable) periodic points are centres of stretching and folding in the flow. The flow with rotation angle $\theta = \pi$ (Figure 1(b)) can be regarded as *more chaotic*. It contains only two relatively large (period-2) islands in the bulk of the flow domain. The protocol with $\theta = 2\pi$ (Figure 1(c)) results in an almost globally chaotic flow, with no noticeable islands. It seems, however, that all chaotic flows belonging to this family of protocols have thin regular layers adjacent to both cylinders. In case of $\theta = 2\pi$ a stable (elliptic) periodic point was detected near the inner cylinder—its position is shown in Figure 1 by the non-filled circular marker. Note that the islands that are not single connected (in this flow they enclose the inner cylinder) do not necessarily have to contain a periodic point of appropriate order inside the island itself.

This paper discusses some numerical aspects of a 'new' method, the mapping method, to study chaotic mixing flows. The first part deals with the eigenvalues of the mapping matrix; the second part studies interface stretching for different grid sizes.

2. BASICS OF MAPPING METHOD

2.1. The original mapping technique

The flow domain Ω is divided into N non-overlapping sub-domains Ω_i, with boundaries $\partial\Omega_i$, and the mixture is described with coarse-grain concentration C, within each cell. The column vector containing all the cell values at time t_k is $\{C\}^k$. The mapping method, based on ideas suggested by Spencer and Wiley [9], advances these values over large, discrete time steps using a matrix multiplication:

$$C_i^{k+1} = \sum_{j=1}^{N} \Phi_{ij} C_j^k \tag{1}$$

The *mapping matrix* Φ is constructed using the velocity field in the flow domain and an accurate adaptive interface tracking algorithm [3]. To obtain the mapping matrix the boundaries $\partial\Omega_i$ of the grid cells Ω_i are tracked from the time t_k to t_{k+1}. This deformed grid is then laid over the initial grid, and each matrix component Φ_{ij} is computed as the area of overlap between deformed cell j and undeformed cell i, divided by the total area of cell i:

$$\Phi_{ij} = \int_{\Omega_j|t_{k+1} \cap\ \Omega_i|t_k} \mathrm{d}\Omega \Big/ \int_{\Omega_i|t_k} \mathrm{d}\Omega \tag{2}$$

The resulting matrix can be very large (in the examples of this paper it has 3.6×10^9 elements), but is normally essentially *sparse* [6].

First, properties of the eigenvalues of the mapping matrix and their corresponding eigenvectors are discussed. As these vectors actually describe the field of concentration, we will call them 'eigenmodes'. Note that, while real eigenmodes describe the concentration distribution (or its perturbation, as we will see later), the physical meaning of complex eigenmodes is not clear. The following simple linear norm for the real positive distribution vector C, defined as

$$M(C) = \sum_{i=1}^{N} C_i S_i \tag{3}$$

where S_i is the area of the cell number i, determines the total volume of the fluid that corresponds to this concentration distribution. For brevity we will refer to such a norm as the *mass* of the distribution (eigenmode), including the cases of any type of eigenmodes. The mapping transformation preserves the mass of the fluid, thus it can be shown that for *any* distribution C the norm $M(C)$ is preserved,

$$M(\Phi C) = M(C) \tag{4}$$

since the mapping, defined by Equations (1) and (2) merely redistributes all the fluid in the system.

This mass conservation has an interesting implication for the eigenvalues and associated eigenmodes. If C_λ is an eigenmode associated with eigenvalue λ, it means that

$$\Phi C_\lambda = \lambda C_\lambda \tag{5}$$

Since the norm M is linear,

$$M(\Phi C_\lambda) = M(\lambda C_\lambda) = \lambda M(C_\lambda) \tag{6}$$

Taking into account Equation (4) we get

$$\lambda M(A) = M(A) \tag{7}$$

Thus, for any eigenvalue such that $\lambda \neq 1$ we necessarily obtain that the mass of the corresponding eigenmode must be equal to zero. Such an eigenmode with zero norm can be considered as a perturbation applied to a uniform concentration distribution. The magnitude of $|\lambda|$ then controls the rate of decay of this perturbation. There is always one eigenvalue $\lambda = 1$ that corresponds to a uniform distribution. Ideally, if there are other eigenvalues with $|\lambda| = 1$ they describe non-decaying modes associated with zones of the flown between which there is no material exchange. Some of these zones represent regular islands, other correspond to isolated chaotic regions (it is possible to have different chaotic regions, which do not exchange material).

The meaning of the complex eigenvalues and eigenmodes may be explained by the following considerations. Suppose that there is a system with n islands of period n and the grid is ideally fitted to them: islands boundaries coincide with the cell boundaries (thus, no numerical diffusion). We assume that there are eigenmodes responsible for these islands. Since after n mappings the distribution must be completely recovered, we get $\lambda^n = 1$. This gives us the possibility to think that there are n eigenvalues: namely the nth-order complex roots of 1. As the simplest example, negative real eigenvalues can correspond to second-order periodicity, since $(\pm 1)^2 = 1$ (here we are considering *all* complex roots).

If the boundaries of the mapping sub-domains do not match exactly with the boundaries of these isolated zones, numerical diffusion will cause the gradual erasing of the perturbation. Thus, computed eigenvalues will have absolute values less than 1. Slow decay of the disturbance ($|\lambda|$ close to 1) still can serve as an indication of rather slow exchange between different zones of the flow.

2.2. The extended mapping method

A useful interfacial area measure, which includes orientation, is the *area tensor* [10]. The second-order area tensor $\mathbf{A}$ is defined as

$$\mathbf{A} = \frac{1}{V} \int_{\Gamma} \mathbf{nn} \, \mathrm{d}\Gamma \tag{8}$$

The components of the area tensor have units of interfacial area per unit volume, and the trace of the tensor equals the total interfacial area per unit volume

$$\operatorname{trace} \mathbf{A} = S_V \tag{9}$$

so $\operatorname{trace} \mathbf{A}$ is a useful scalar measure of microstructural mixing. The averaging volume V should be large enough to provide a representative sample of the microstructure, but smaller than the scale over which the microstructure varies. The extended mapping method now updates the area tensor at each time step according to

$$\mathbf{A}_i^{k+1} = \sum_{j=1}^{N} \Phi_{ij} (\mathbf{A}_j^k \otimes \mathbf{F}_{ij}^{-1}) \tag{10}$$

That is, the area tensor in any cell at time $k+1$ is the sum of contributions from all donor cells, after the donor tensors from time k have been transformed by the appropriate

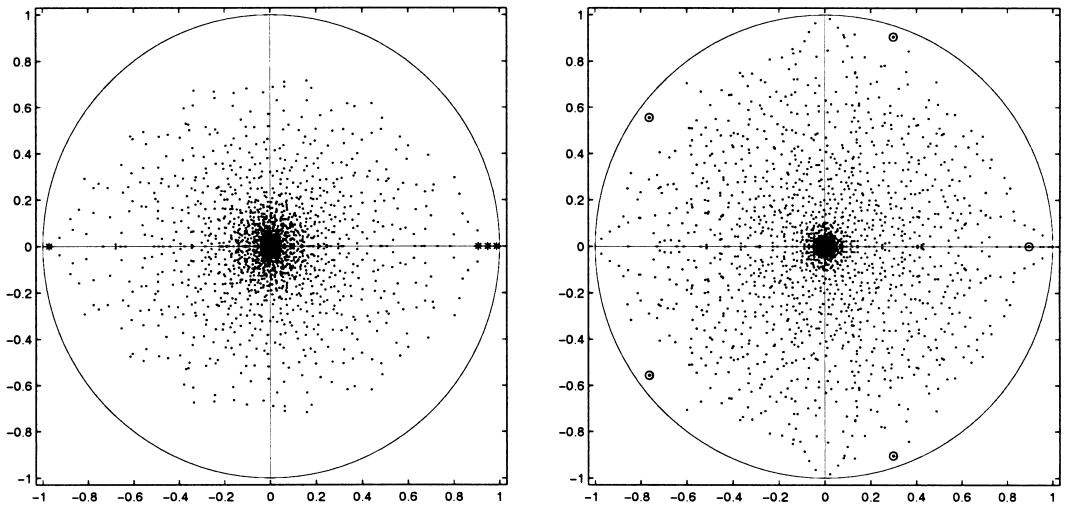

Figure 2. (a) The eigenvalues of the full-period mapping matrix for the flow with $\theta = \pi$ and $\Omega = 3$. (b) Eigenvalues for $\theta = 0.5\pi$. The five eigenvalues correspond to a system of period-5 islands are marked with circles.

deformation gradients. The symbol $\otimes$ denotes the transformation of the area tensor under finite strain which converts an initial area tensor $\mathbf{A}^0$ to an equivalent *droplet shape tensor* [2] $\mathbf{G}^0$, finds the droplet shape tensor $\mathbf{G}$ in the deformed state, and then transforms $\mathbf{G}$ back to find the deformed-state area tensor $\mathbf{A}$. Equations (10) and (1) constitute one step of the extended mapping method. All details of the conversion between $\mathbf{A}$ and $\mathbf{G}$ and on the validation of the extended mapping method can be found in Reference [2].

3. RESULTS

3.1. Eigenvalues and eigenvectors for mapping matrices

We consider the mapping matrices for the *full period* of the flows with $\Omega = 3$ and $\theta = \pi$ and 0.5π, respectively. Unlike the rest of the paper, a rather coarse grid, containing only 2400 sub-domains is used. This makes it possible to compute all eigenvalues and, if necessary, the corresponding eigenvectors. Figure 2(a) shows the location in the complex plane of all the eigenvalues of the full-period mapping matrix for the flow with $\theta = \pi$ and $\Omega = 3$. We focus on the real eigenvalues with the largest absolute values.

First, an eigenvalue $\lambda_0 = 1$ is observed that corresponds to a trivial eigenmode $C_i = \text{const}$ describing a uniform density distribution. We also examined few other real eigenmodes with large absolute values. They provide some essential information about the material transport in the flow under study. Figure 3 shows the eigenmodes, corresponding to the values $\lambda_1 = 0.9867$, $\lambda_2 = 0.9071$ and $\lambda_3 = -0.9722$.

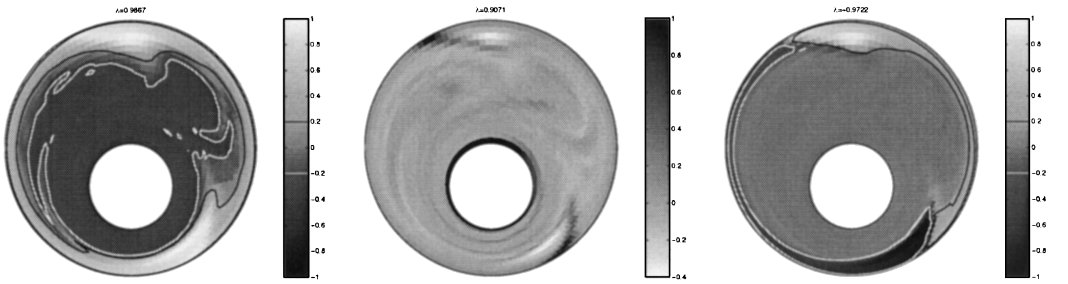

(a) (b) (c)

Figure 3. The real eigenmodes (perturbation of concentration) of the full-period mapping matrix for the flow with $\theta = \pi$ and $\Omega = 3$. The eigenmodes correspond to the eigenvalues: (a) $\lambda_1 = 0.9867$, (b) $\lambda_2 = 0.9071$, (c) $\lambda_3 = -0.9722$.

The slowest-decaying eigenmode, which corresponds to $\lambda_1 = 0.9867$, is shown in the Figure 3(a). It demonstrates that there is only very slow exchange of material between the wide ring adjacent to the outer cylinder and the rest of the flow domain. From the Poincaré map (Figure 1(b)) is known that this ring contains two period-2 islands. It was suggested above that periodic structures of the second order should reveal themselves through the presence of the real eigenvalue close to -1. Figure 3(c) shows the eigenmode that corresponds to $\lambda_3 = -0.9722$. Bright and dark regions in the plot, corresponding to positive and negative values of concentration disturbance, are clearly seen in the outer layer of the flow domain. Since the eigenvalue $\lambda_3 = -0.9722$ is negative, the material contained in these two zones is being swapped after each period of the flow. The eigenmode that corresponds to $\lambda_2 = 0.9071$ is shown in Figure 3(b). It indicates that there is also a zone around inner cylinder that exchanges material with the rest of the domain rather slowly. The Poincaré map in Figure 1(b) shows that there is actually a thin ring-shaped island enclosing the inner cylinder. We can see that eigenmodes of real eigenvalues of the full-period mapping matrix can indeed reveal the nearly isolated zones of the flow.

Since higher-order periodicity is associated with complex eigenvalues, it is of interest to examine the flow with $\theta = 0.5\pi$ and $\Omega = 3$, because it contains the system of five islands of fifth order, revealed by the Poincaré map (Figure 1(a)). The corresponding mapping matrix in fact possesses eigenvalues close to the complex roots $\sqrt[5]{1}$. These eigenvalues, marked with circles in Figure 2(b), are situated near the vertices of a regular pentagon. The real parts or absolute magnitude of the corresponding eigenmodes indicate that these eigenvalues are related to the above-mentioned period-5 islands.

The eigenvalue pattern also shows four distinct 'leaflets' of high absolute values near the real and imaginary axes. We believe that these leaflets are caused by a behaviour close to fourth-order periodicity in the outer ring of the flow domain. This becomes clear if we notice that actually every point on the outer boundary returns to its original location after four periods, since $\theta = 0.5\pi$.

Comparing the two plots in Figure 2 we can see that for the flow with $\theta = \pi$ the eigenvalues are grouped more densely around the origin $(0, 0)$. This serves as an indication that most of the perturbation in this flow decays faster than in the flow with $\theta = 0.5\pi$.

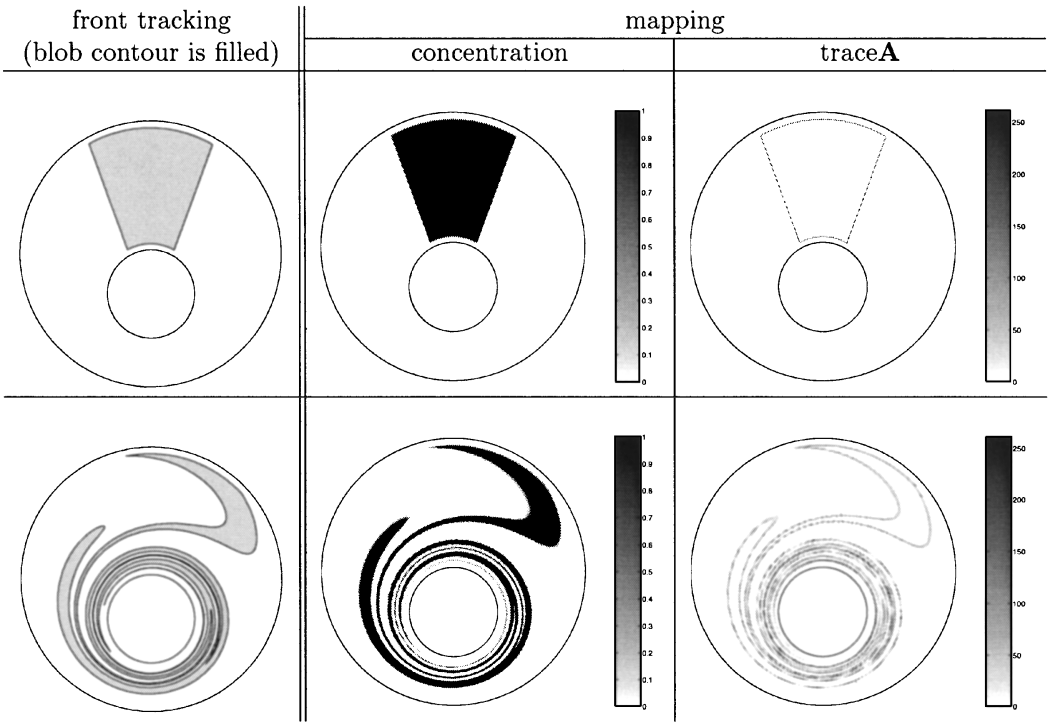

Figure 4. Comparison of the mapping and front tracking results. Top row shows initial distributions, bottom—after one period of the flow with $\theta = 2\pi$ and $\Omega = 3$.

3.2. *Interfacial area generation*

The deformation of a blob, depicted in the upper row of Figure 4 was computed for three different flows with $\theta = 0.5\pi$, π and 2π (in all three cases $\Omega = 3$) by using both front tracking and the extended mapping approach. The total length of the interface was recovered from the mapping results as a sum over all sub-domains (cells):

$$L = \sum_{i=1}^{N} S_i \operatorname{trace} \mathbf{A}_i \tag{11}$$

when $\mathbf{A}_i$, is the area tensor in the sub-domain number i that has an area equal to S_i.

Figure 4 compares the mapping and tracking simulations. The concentration, plotted in the middle, is captured quite well by the mapping method. The plots on the right show the extended mapping results, in particular trace **A**. The interface is captured remarkably accurately. Figure 5 shows quantitative comparisons for mapping and tracking for different mapping grids. Consistency of the mapping method is shown to be independent on the rotation angle θ. The prediction of interfacial area is very accurate for the journal bearing flow. In previous work [2], mixing in the rectangular lid-driven cavity flow was studied and there the prediction of the growth of interfacial area was significantly less accurate and over-predicted due to the presence of corner singularities.

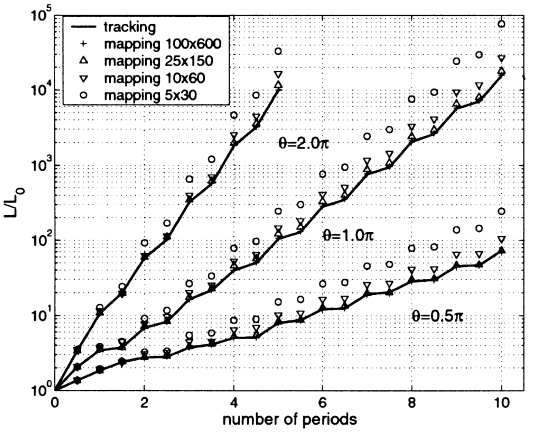

	$L/L_0 \times 10^4$		
Period	1.0	3.0	5.0
tracking	0.00106	0.0325	1.0041
100×600	0.00106	0.0333	1.0031
50×300	0.00108	0.0321	1.0123
25×150	0.00109	0.0343	1.1570
10×60	0.00115	0.0399	1.6409
5×30	0.00126	0.0653	3.2934

Figure 5. Left: interface stretching obtained using front tracking and extended mapping technique for different mapping grids and $\theta = 0.5\pi$, π, and 2π. On the right, quantitative comparisons are shown for $\theta = 2\pi$.

4. CONCLUSIONS

The paper discusses numerical aspects of the mapping method. The first part of the paper considers the eigenvalues of the mapping matrix for two different journal bearing flows. Numerical results reveal different zones of mixing via the eigenmodes, and the rate of mixing follows from the corresponding eigenvalues.

In the second part of the paper numerical results for the extended mapping method are presented. Accuracy of the technique is shown by comparison with front tracking results for different grids. Interface stretching is calculated accurately even on rather coarse grids, and consistency of the technique is demonstrated.

REFERENCES

1. Aref H, Balachandar S. Chaotic advection in a Stokes flow. *Physics of Fluids* 1986; **29**:3515–3521.
2. Galaktionov OS, Anderson PD, Peters GWM, Tucker III CL. A global, multi-scale simulation of laminar fluid mixing: the extended mapping method. *International Journal of Multiphase Flows* 2002; **28**(3):497–523.
3. Galaktionov OS, Anderson PD, Peters GWM, van de Vosse FN. An adaptive front tracking technique for three-dimensional transient flows. *International Journal for Numerical Methods in Fluids* 2000; **32**:201–218.
4. Joukowski NE. Motion of a viscous fluid contained between rotating eccentric cylindrical surfaces. *Proceedings of the Khar'kov Mathematical Society* 34–37, 1887 (in Russian) (German abstract *Jb Fortschr. Math.* **19**, 1019).
5. Joukowski NE, Chaplygin SA. Friction of a lubricated layer between a shaft and its bearing. *Trudy old fiz nauk obshch. Lyub. Estest.* 1904; **13**:24–36 (in Russian) (German abstract *Jb Fortschr. Math.* **35**, 767).
6. Kruijt PGM, Galaktionov OS, Anderson PD, Peters GWM, Meijer HEH. Analysing fluid mixing in periodic flows by distribution matrices: the mapping method. *AIChE* 2001; **47**(5):1005–1015.
7. Muzzio FJ, Swanson PD, Ottino JM. The statistics of stretching and stirring in chaotic flows. *Physics of Fluids A* 1991; **3**:822–834.
8. Ottino JM. *The Kinematics of Mixing*: *Stretching*, *Chaos and Transport.* Cambridge Texts in Applied Mathematics, Cambridge University Press: Cambridge, 1989.
9. Spencer RS, Wiley RH. The mixing of very viscous liquids. *Journal of Colloid Science* 1951; **6**:133–145.
10. Wetzel ED, Tucker CL. Area tensors for modeling microstructure during laminar liquid–liquid mixing. *International Journal of Multiphase Flows* 1999; **25**:35–61.

